Journal of Molecular Graphics and Modelling 124 (2023) 108565

Contents lists available at ScienceDirect

Journal of Molecular Graphics and Modelling

journal homepage: www.elsevier.com/locate/jmgm

Identification of novel compounds against *Acinetobacter baumannii* 3-oxoacyl-[acyl-carrier-protein] synthase I (FabB) via comprehensive structure-based computational approaches☆

Esra Albayrak [a], Sinem Koçer [b], Ozal Mutlu [a,*]

[a] Marmara University, Faculty of Science, Department of Biology, Goztepe Campus, 34722, Kadikoy, Istanbul, Turkey
[b] Istanbul Yeni Yuzyil University, Faculty of Pharmacy, Department of Pharmaceutical Biotechnology, 34010, Cevizlibag, Istanbul, Turkey

ARTICLE INFO

Keywords:
Acinetobacter baumannii
3-Oxoacyl-[acyl-carrier-protein] synthase I
FabB
Computer-aided drug discovery
Molecular dynamics simulation

ABSTRACT

Acinetobacter baumannii is one of the most serious opportunistic pathogens according to WHO. The difference between bacterial and mammalian fatty acid biosynthesis pathways makes FASII enzymes attractive targets in drug discovery. 3-oxoacyl-[acyl-carrier-protein] synthase I (FabB) from the FAS II pathway catalyze the condensation of malonyl ACP with acyl-ACP, and elongates the fatty acid chain by two carbons. To investigate potential inhibitors of the *A. baumannii* FabB, we used computational approaches including homology modeling, high-throughput virtual screening, molecular docking, molecular dynamics simulations, and MM-GBSA free energy calculations. After the high-throughput virtual screening, the resulting ligands were further screened using the *QM-polarized ligand docking (QPLD) and induced fit docking (IFD)* approaches. Molecular dynamics simulations were performed for 100 ns. And according to binding free energy calculations, we have identified nine compounds with the best binding affinities. Three of these compounds were selected for an additional 1 μs MD simulation to assess ligand stability. Two of them named L6 and L7 showed promised stability and affinity to the target. Here, we present novel compounds against *A. baumannii* FabB via structure-based computational approaches. These compounds might pave the way for the design of new lead structures and inhibitors for multidrug-resistant *A. baumannii*.

1. Introduction

Antibacterial resistance is an emerging threat to global healthcare, and it is estimated that the number of annual deaths caused by antibacterial resistance, will be ten million by 2050 [1]. Furthermore, multidrug-resistant bacterial infections, known as 'superbug' infections, are responsible for serious diseases in humans [2,3]. World Health Organization (WHO) has released a global priority list that includes 12 pathogens such as *Enterococcus faecium, Staphylococcus aureus, Klebsiella pneumoniae, Acinetobacter baumannii, Pseudomonas aeruginosa*, and *Enterobacter* species [4]. These six most drug-resistant nosocomial pathogens are also known as ESKAPE pathogens [5]. WHO also described these pathogens in three categories: critical, high, and medium. Carbapenem-resistant *A. baumannii* was presented in the critical priority group and reported as an urgent threat by the Centers for Disease Control and Prevention (CDC) [4,6]. According to European Centre for Disease Prevention and Control, 12 out of 27 countries reported the *A. baumannii* carbapenem resistance rate of 50% or higher for more than 10 isolates [7]. Studies demonstrated that the crude mortality rate of *A. baumannii* infection is between 40% and 80%. In the Mediterranean region, multidrug-resistant *A. baumannii* has the highest carbapenem resistance, which is 90% [8]. The intensive care unit mortality rate caused by *A. baumannii* was reported to be 84.3% [9].

As a result of differences in the cell wall compositions, Gram-negative bacteria infections, including opportunistic pathogen *A. baumannii*, are more difficult to treat than Gram-positive bacteria. Due to its multidrug-resistance to carbapenem, penicillin, cephalosporins, fluoroquinolones, and aminoglycosides agents, *A. baumannii* has become an interesting research focus on developing novel antibiotics [10]. Bacterial fatty acid biosynthesis enzymes are particularly attractive targets for novel drug candidates because of their differences from their mammalian counterparts [11]. There are two types of fatty acid

☆ This research did not receive any specific grant from funding agencies in the public, commercial, or not-for-profit sectors.
* Corresponding author.
E-mail address: ozal.mutlu@marmara.edu.tr (O. Mutlu).

https://doi.org/10.1016/j.jmgm.2023.108565
Received 25 April 2023; Received in revised form 18 June 2023; Accepted 10 July 2023
Available online 12 July 2023

synthetic (FAS) pathways: type I fatty acid synthase of mammals, fungi, and lower eukaryotes and type II fatty acid synthase of prokaryotes, and plastids [12]. The FAS II pathway initiates with fatty acid biosynthesis (Fab) enzyme D, FabD, acting as a malonyl CoA-ACP transacylase and converting the malonyl-CoA to malonyl-ACP. Subsequently, FabH condenses malonyl-ACP and acetyl-CoA to the first cycle β-ketoacyl-ACP and initiates the elongation cycle. Next, β-ketoacyl-ACP is transformed into β-hydroxyacyl-ACP by the enzyme FabG. Followed, β-hydroxyacyl-ACP is dehydrated to *trans*-2-enoyl-ACP by FabZ/FabA. FabI, FabK, FabL, and FabV which are all enoyl-ACP reductase enzymes, produce acyl-ACP molecules from *trans*-2-enoyl-ACP. The elongation cycle is then supported by FabB/FabF enzymes that condense various acyl-ACP substrates and malonyl-ACP to β-ketoacyl-ACP [2]. Thus, condensing enzymes are required for the critical and irreversible elongation step of fatty acid biosynthesis [13,14]. In terms of the active site structure, three different enzymes from the FAS II pathway, FabB, FabF, and FabH, display similarities. Highly conserved ACP's active sites contain a central cysteine residue in the catalytic triad. Both FabB and FabF have a Cys/His/His catalytic triad, Cys163/His298/His333, and Cys163/His303/His340 respectively, while FabH has a Cys/His/Asn catalytic triad, Cys112/His244/Asn274 (*Escherichia coli* numbering) [15–18].

Antibacterial compounds interacting with enzymes of the FAS II pathway can inhibit lipid synthesis, which is essential for cell viability, and membrane integrity and relevant for pathological virulence [13,19]. To date, some inhibitors of condensing enzymes have been identified. Previous studies have shown that cerulenin is an irrevocable inhibitor of FabB and FabF. It forms a covalent bond with the central cysteine in the triad (Cys163) and its O-2 forms hydrogen bonds with both histidines in the active site of FabB (His298 and His333) [13]. Cerulenin also inhibits the mammalian FAS I pathway, which makes it a potential inhibitor for the mammal's fatty acid pathway. Moreover, *in vivo* analysis showed that cerulenin significantly reduced body weight in mice [13,20]. Due to cysteine-reactive epoxide group activity and chemical instability, cerulenin has been excluded from clinical development [21]. Thiolactomycin (TLM) is also an inhibitor of FabB and FabF and forms hydrogen bonds with active site histidines (His298 and His333) in the malonyl-ACP binding site. However, TLM is a more sensitive inhibitor of FabF than FabB, while it shows the lowest affinity to FabH, which is calculated as 158 μm [13]. Slow onset inhibition of TLM is reversible and Fab enzymes can be protected by existing malonyl-ACP [13,22]. Also, missense mutations and overexpression of FabB cause TLM resistance [23,24]. Platensimycin (PTM) and its analog platencin (PTN) inhibit the FabF/B and FabF/FabH respectively. Both molecules exhibit antibacterial activity against gram-positive bacteria [25,26]. Due to efflux mechanisms in gram-negative bacteria, PTM efficacy is probably restricted for also *A. baumannii*. PTM may not be capable of inhibition unless these pump mechanisms mutate or by using a second drug to block the pumps [25,27].

In this study, novel compounds against the multidrug-resistant *A. baumannii* FabB (AbFabB) enzyme were identified. The structure of the enzyme was generated via homology modeling and then structure-based and computer-aided drug discovery approaches were used. After high-throughput virtual screening and several docking campaigns, the stability of the resulting compounds was analyzed using molecular dynamics simulations, and the free energy of binding was calculated. As a result, two compounds with low binding free energies and high stability were selected as potential inhibitory molecules.

2. Materials and methods

2.1. Protein modeling and validation

The FabB amino acid sequences from *Yersinia pestis* (Accession number: WP_002209717.1 and PDB ID: 3OYT) [28], Escherichia *coli* (Accession number: NP_416826.1 and PDB ID: 1G5X) [29], *Brucella melitensis* (Accession number: WP_002965234.1 and PDB ID: 3LRF) [30], *Vibrio cholera* (Accession number: WP_000832701.1 and PDB ID: 4XOX) [31] and *Pseudomonas aeruginosa* (Accession number: WP_003087471 and PDB ID: 7PPS) [32] were retrieved from the NCBI database (https://www.ncbi.nlm.nih.gov) and the RSCB Protein Data Bank (PDB) (www.rcsb.org). The multiple sequence alignments of FabB sequences were carried out by using the MUSCLE (http://www.ebi.ac.uk/Tools/msa/muscle) program and visualized via ESpript 3.0 (https://espript.ibcp.fr/ESPript/cgi-bin/ESPript.cgi) [33,34]. The amino acid sequence of AbFabB was obtained from the NCBI Protein database (Accession no: BAN89261). AbFabB was modeled by using the SWISS-MODEL web server (https://swissmodel.expasy.org/) [35]. In addition; the AlphaFold model of AbFabB was obtained from the AlphaFold Protein Structure Database (https://alphafold.ebi.ac.uk) [36,37]. Quality check of the models was performed with PROCHECK, ERRAT, ProSA, and Verify3D programs [38–41]. PROCHECK was used to generate the Ramachandran plot of the AbFabB models [38]. The statistics of protein model atom interactions were analyzed by ERRAT [39]. ProSA and Verify3D were utilized to examine the 3-dimensional structural model quality [40,41]. Protein models and the template structure were superimposed based on C-alpha atoms with PyMOL (The PyMOL Molecular Graphics System, Version 2.3.2 Schrodinger, LLC). AbFabB secondary structure elements were estimated and visualized by using PDBsum [42,43]. Functional domain prediction was performed using the amino acid sequence of AbFabB with the Pfam web server [44]. The Expasy ProtParam tool was utilized to predict the physicochemical properties of AbFabB (http://web.expasy.org/protparam) [45].

2.2. Virtual screening, quantum-polarized ligand docking, and induced fit docking

Drug-Like green collection of OTAVAchemicals (OTAVA Ltd., Canada) including about 170.000 compounds was used in the virtual screening. The ligand library was prepared by using the LigPrep program (LigPrep, Schrödinger, LLC, New York, NY, 2021). The protein structure was prepared by assigning the bond orders, adding H atoms and optimizing at pH 7.0, and applying a short step of energy minimization using the Protein Preparation Workflow (Protein Preparation Wizard; Epik, Schrödinger, LLC, New York, NY, 2021; Impact, Schrödinger, LLC, New York, NY, 2021; Prime, Schrödinger, LLC, New York, NY, 2021). The virtual screening was conducted using the Glide virtual screening workflow (Glide, Schrödinger, LLC, New York, NY, 2021) applying the high-throughput virtual screening (HTVS), standard precision (SP), and extra precision (XP) docking modes respectively. In the HTVS and SP campaigns, 10% of the compounds were selected for the next stage. At the end of the virtual screening workflow (XP mode), the 100 best compounds were ranked according to the XP GScores. Visual inspection was carried out for the interaction with catalytic residues His349, His313, and Cys174. In addition, another selection was performed according to ADME values and Lipinski's rule of five, and low-value compounds were discarded (QikProp, Schrödinger, LLC, New York, NY, 2021) [46]. Then, the quantum-polarized ligand docking (QPLD) protocol was used to select ligands by using the XP docking mode at the initial and final selection stages. QM charges were calculated by accurate mode (uses the 6-31G*/LACVP* basis set, B3LYP density functional, and "Ultrafine" SCF accuracy level). The final selection was made according to the Emodel energies of the poses (QM-Polarized Ligand Docking protocol; Glide, Schrödinger, LLC, New York, NY, 2020; Jaguar, Schrödinger, LLC, New York, NY, 2021; QSite, Schrödinger, LLC, New York, NY, 2021). In the final stage, induced-fit docking (IFD) was performed with the selected compounds, where both the ligand and the active site residues were allowed to be flexible (Induced Fit Docking protocol; Glide, Schrödinger, LLC, New York, NY, 2021; Prime, Schrödinger, LLC, New York, NY, 2021). The known FabB inhibitor thiolactomycin (TLM) was also docked for comparison using the same procedure as the other compounds.

2.3. Molecular dynamics simulations and binding free energy calculation

Molecular dynamics simulations of the protein-ligand (including inhibitor thiolactomycin) and apo-protein structures were performed by using the Desmond program (Desmond Molecular Dynamics System, D. E. Shaw Research, New York, NY, 2021. Maestro-Desmond Interoperability Tools, Schrödinger, New York, NY, 2021). In all steps, the OPLS4 forcefield was used [47]. An orthorhombic box filled with the SPC waters was built and after the neutralization, ionic strength was adjusted to 0.15 M with Na^+ and Cl^- ions [48]. In the beginning, 100 ps of minimization and default relaxation protocol were applied to prepare the system for the production run. Then the simulation was run in the NPT (isobaric-isothermic) ensemble class at 300 K and 1 bar pressure for 100 ns or 1 μs. Trajectories were recorded every 50 ps and 125 ps time intervals for 100 ns and 1 μs simulations, respectively. For both 100 ns and 1 μs simulations, the time step was 2.0 fs. Nose-Hoover Chain thermostat and Martyna-Tobias-Klein (MTK) barostat with isotropic coupling style were used and the coulombic cut-off radius was set to 9.0 Å [49]. GPU-based and CPU-based computing was conducted using the Intel i7-7700 3.60 GHz and 32 GB RAM system equipped with the NVIDIA GTX 1060 3 GB graphic card. The simulation interaction diagram panel was used to analyze protein RMSD (root mean square deviation) and RMSF (root mean square fluctuation), ligand RMSD (ligfitlig and ligfitprotein), protein-ligand contacts, and ligand properties. The binding energy of the compounds was calculated for each snapshot of the simulation using the Prime program (Prime, Schrödinger, LLC, New York, NY, 2021) and the *thermal_mmgbsa.py* script designed for MM-GBSA ΔG binding calculation with the following equation:

MM-GBSA ΔG Bind = E_Complex – (E_Receptor + E_Ligand)

During the selection of compounds for the next step, ΔG binding free energies and interaction with catalytic residues were considered.

3. Results and discussion

3.1. Overall structure of AbFabB

FabB from *Vibrio cholerae* (PDB ID: 4XOX) was selected as a template structure with 57.46% identity for the homology modeling. After modeling, GMQE (Global Model Quality Estimate) and QMEAN scores were determined as 0.82 and −1.13, respectively. Validation analyses were carried out by using the PROCHECK, ERRAT, ProSA, and Verify3D programs [38–41]. The Ramachandran plot revealed that 88.7%, 9.9%, and 0.6% of the residues were in the most favored regions, allowed regions, and generously allowed regions, respectively (Supplementary Fig. S1). The overall quality factor of the model was calculated as 93.233% in the ERRAT program (Supplementary Fig. S2). PROSA Z-score of the AbFabB model was −9.93 and the model was found to be similar to the protein structures solved by X-ray crystallography (Supplementary Fig. S3). VERIFY3D showed that 97.31% of the amino acid residues had averaged 3D-1D scores (Supplementary Fig. S4). The RMSD value between the template and the homology model structure was found to be 0.095 Å (over 358 atoms) with respect to C-alpha traces (Supplementary Table S1).

On the other hand, several validation scores are very similar for the models obtained from the Swiss-Model and the Alpha-Fold (Supplementary Table S1). Ramachandran plot results for the AlphaFold model of AbFabB showed that 91.0%, 8.2%, and 0.5% of the residues were in the most favored regions, allowed regions, and generously allowed regions, respectively. The overall quality factor of the model was found to be 94.5946 and PROSA Z-score was −9.88 for the AlphaFold model of AbFabB. However, the VERIFY3D score of the AlphaFold model was found to be 79.86%, slightly below of threshold value (80%). In addition, the RMSD value between the template and the AlphaFold model was calculated as 0.524 Å (over 333 atoms) with respect to C-alpha traces. The overall structural conformation of the AbFabB homology model was observed to be closer to the crystal structure of the template protein than the AlphaFold model. In some benchmark studies, it was emphasized that the AlphaFold models may have low model quality, and therefore, studies should be carried out to increase accuracy [50,51]. A comparison study also reported that the Alpha-fold model did not perform well in high-throughput docking analyses [52]. Taken together; validation results show that the homology model of AbFabB is of good quality and suitable for the structure-based screening studies at the next stage.

Primary structure analysis of AbFabB was performed by multiple sequence alignment using FabB amino acid sequences from *Y. pestis, E. coli, B. melitensis, V. cholera, and P. aeruginosa* (Fig. 1). AbFabB showed 50.62%; 51.49%; 50.50%; 56.97%; and 54.84% identities with *Y. pestis, E. coli, B. melitensis, V. cholera, and P. aeruginosa*, respectively. In the alignment, Cys-His-His active site triad is also observed to be conserved in AbFabB compared to FabB proteins whose crystal structure is resolved. The Cys residue in the active site (Cys174 in AbFabB) is responsible for substrate binding and accepts the acyl group from the acyl-ACP [30,53,54]. In a recent study, *P. aeruginosa* FabB Cys161 was mutated to Ala, and it was observed that this mutation ensured Phe391 became in the open conformation, making the enzyme a target that allows entering inhibitors. In this way, the study revealed the importance of this residue (Cys174 in AbFabB) in drug design [32]. The two histidine residues (His313 and His349 in AbFabB) are involved in nucleophilic activation following malonyl-ACP binding [30,54]. These histidine residues have also been known to play an important role in protein-drug interaction [13]. In addition, the Phe408 residue that is highly conserved is responsible for substrate specificity and facilitates the entry of the substrate into the binding site in the open conformation of the enzyme [30,53].

The secondary structure of AbFabB was predicted to consist of 15 α-helices and 14 β-strands. The thiolase-like αβαβα fold in β-ketoacyl-ACP-synthases is also located in AbFabB (Figs. 1 and 2) [30,53]. The two β-strand groups were shown in Fig. 2B. Structure domain prediction of AbFabB was carried out by the Pfam web server [44]. N-and C-terminal domains of beta-ketoacyl synthase in the keto-acyl synthase family were found to be associated with AbFabB at e-values $2.7e^{-39}$ and $8.2e^{-31}$ respectively.

The physicochemical properties of AbFabB were also analyzed. The molecular weight of the enzyme is about 44.87 kDa, theoretical pI is 5.45, AbFabB has 47 negative and 36 positively charged residues, extinction coefficient is 30745, the aliphatic index is 86.52 and grand average of hydropathicity is −0.041 according to ProtParam tool results.

3.2. Molecular docking, molecular dynamics simulations, and free-energy calculation

Virtual screening was conducted in the malonyl (Acyl)-ACP binding site of the AbFabB by using the drug-like green collection of OTAVAchemicals (OTAVA Ltd., Canada) including about 170.000 compounds that obey Lipinski's rules of five [46]. At the end of the virtual screening, we ended up with the 100 highest rated compounds selected according to the XP GScore. Every docking pose was visually inspected for the interaction with the active site residues His349, His313, and Cys174, and 88 compounds were selected for the ADME analysis. Compounds with low ADME properties including Caco cell permeability and human oral absorption were eliminated. Subsequently, the resulting compounds were evaluated using QM polarized ligand docking to improve docking accuracy and then analyzed by induced fit docking, which allows both the active site residues and ligands to change conformation. Finally, the top 10 compounds having the best IFD scores were evaluated by molecular dynamics simulations for 100 ns to assess ligand stability and to calculate end-point binding free-energy by using the Prime MM-GBSA (Molecular mechanics with generalized Born and surface area solvation) method. During the MD simulations, the top nine

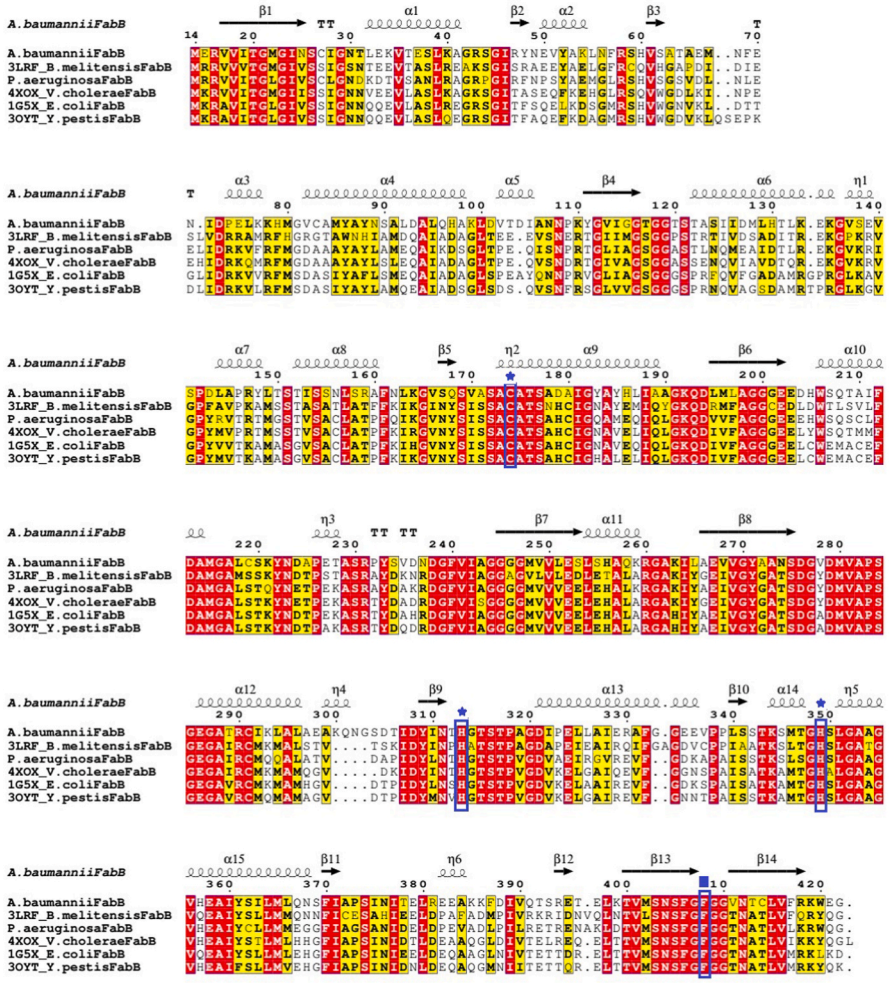

Fig. 1. Multiple sequence alignment of AbFabB with FabB sequences from *Y. pestis*, *E. coli, B. melitensis, V. cholera,* and *P. aeruginosa.* Cys-His-His active site triad is marked by an asterisk and the Phe408 residue is marked by a square. β-Sheets are shown in arrows; α-helices are shown in helices.

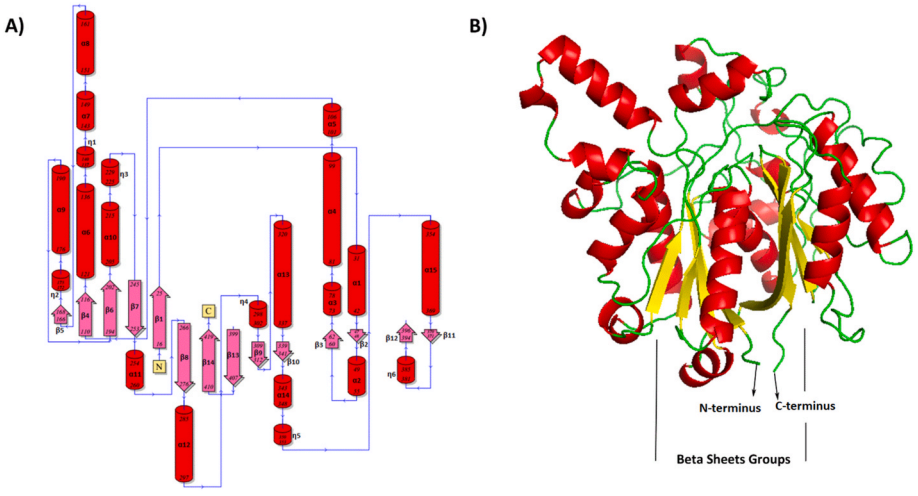

Fig. 2. Representation of *A. baumannii* FabB structural models. A) Topology model of the secondary structure of AbFabB. B) Three-dimensional structure of AbFabB.

compounds with good ΔG energies were identified that interact with active site residues (Table 1). The ADME properties of the selected ligands are also given in Supplementary Table S2.

According to the molecular docking scores, compounds have lower XP GScores in IFD than the HTVS and QPLD campaigns (Table 1). We have also docked the thiolactomycin (TLM) inhibitor for comparison with the compounds. We obtained a similar binding pose found in the *E. coli* FabB-TLM complex (PDB ID: 2VB8) where interaction with the active site residues Cys174, His313, and His349 occurred [55]. However, docking scores of TLM are unsatisfactory when compared with our

Table 1
Docking scores and MM-GBSA ΔG binding energies of the top 9 compounds and TLM were selected after the 100 ns of molecular dynamics simulations.

Compound No	Compound Catalog number	HTVS	QPLD	IFD			Prime MM-GBSA	Interacting residues[b]
		XP GScore[a]	XP GScore[a]	XP GScore[a]	Prime Energy[a]	IFDScore[a]	ΔG_Bind[a]	
L1	7013870425	−7.23	−7.164	−10.616	−16466.42	−833.94	−36.72	**His313**
L2	7018801344	−7.119	−6.827	−9.68	−16532.48	−836.3	−47.92	**His313**/His313, **His349, Phe406**/Phe406, Phe408
L3	7020610985	−7.419	−7.326	−9.69	−16523.85	−835.88	−45.54	Phe240, **Val281**, Pro283, Phe406, Phe408
L4	5409960	−6.919	−7.395	−9.025	−16508.32	−834.44	−40.8	**His313**/His313, Phe408
L5	6238550	−7.089	−7.533	−11.16	−16469.52	−834.64	−35.46	**His313, His349**/His349, **Phe406**/Phe406
L6	7564889	−6.976	−7.382	−9.769	−16479.85	−833.76	−61.88	His313, Phe406, **Gly407**
L7	7565285	−6.681	−6.783	−10.276	−16509.43	−835.75	−51.3	**His313, His349**, Phe406, **Gly407**, Phe408
L8	12398517	−6.94	−6.986	−10.366	−16515.62	−836.15	−32.73	**Glu324, His349,** Phe408
L9	7012740234	−7.09	−7.116	−8.85	−16507.26	−834.21	−45.35	Pro283, **Thr315,** Phe406, Phe408
Thiolactomycin (TLM)	135403829[c]	−4.571	ND	−7.507	−16970.96	−856.05	−31.70	**Cys174, His349**

[a] Scores are in kcal/mol.
[b] Residues interacted that more than %50 of simulation time. Bold: H-bond, thin: hydrophobic interaction.
[c] PubChem CID.

hit compounds. The only exception is seen for the IFD score of TLM. Molecular dynamics simulations show that the compounds L1, L2, L4, L5, L7, and L8 make H-bond with at least one catalytic residue (His313 and/or His349), while compound L6 makes hydrophobic interaction (pi-pi stacking with His313). Other than the catalytic residues, Phe406 and/or Phe408 make hydrophobic interactions with the compounds except for L1. Both compounds L2 and L5 have hydrogen bonds and hydrophobic interactions with the Phe406 residue during simulation. Other residues that contribute to protein-ligand interactions are Phe240, Val281, and Pro283 in L3, Gly407 in L6 and L7, Glu324 in L8, Pro283, and Thr315 in L9. The MM-GBSA binding free energies of the protein-ligand complexes varied from −32.73 kcal/mol to −61.88 kcal/mol. L6, the compound with the highest affinity, forms mainly non-polar contacts, while other high affinity compounds (L2 and L7) make polar contacts with the catalytic residues His313 and His349. On the other hand, the simulation of the AbFabB-TLM complex shows that the interaction with His313 is lost while the interaction with Cys174 and His349 is preserved. TLM has the lowest affinity, −31.70 kcal/mol, among compounds that interacted with AbFabB according to the end-point free energy of binding calculation with the Prime (Table 1).

RMSD plot shows changes in the protein structure with respect to the initial position. The average RMSD for the apo-AbFabB protein backbone atoms was found around 1.78 Å. It was shown that there was no major change in the RMSD, and it remained stable through the simulation with minimal variation. The maximum RMSD value for apo-AbFabB was 2.52 Å, while the minimum value was 0.97 Å. The mean RMSD for AbFabB-L1 and AbFabB-L2 complexes were about 1.99 Å. The maximum RMSD value for AbFabB-L1 was 2.78 Å and the system varied between 40 ns and 50 ns for 10 ns and remained stable after 50 ns. The maximum value for the AbFabB-L2 complex was 2.61 Å. Although the mean RMSD AbFabB-L2 was higher than the apo-AbFabB RMSD, there was no significant change in the plot. The mean RMSD for the AbFabB-L3 was 1.87 Å, which is slightly higher than the apo-AbFabB. AbFabB-L4 mean RMSD was 1.95 Å, higher than the apo-AbFabB, and there was a change in the plot before 38 ns. RMSD for the AbFabB-L5 was 1.90 Å and was mostly stable. One of the highest RMSD among the complexes, 2.25 Å, belongs to the AbFabB-L6, and its maximum value was found to be 3.04 Å. The AbFabB-L6 RMSD plot shows similarities after the 77 ns with the apo-AbFabB RMSD plot. AbFabB-L7 mean RMSD was 1.77 Å. Its value is quite similar to apo-AbFabB RMSD. AbFabB-L7 maximum RMSD value, 2.4 Å, lower than apo-AbFabB maximum RMSD value. AbFabB-L8 had a mean RMSD of 1.85 Å, and its most stable value was between 50 ns and 73 ns. For the last complex, AbFabB-L9, the mean RMSD was the same as apo-AbFabB mean RMSD, which is about 1.78 Å. RMSD plot showed that after 38 ns the protein structure remained stable. The RMSD plots and mean RMSD values for 100 ns simulations are represented in Supplementary Fig. S5 and Supplementary Table S3.

RMSF stands for root mean square fluctuation and measures the average flexibility of the residues during simulations based on the reference position. In the plot, the peaks represent the residues that fluctuate the most. Secondary structures like alpha helices and beta strands are more rigid and less fluctuated than the unstructured parts of the protein [56]. For apo-AbFabB, amino acid fluctuations were in an acceptable range and the greatest value of fluctuation was around 5 Å, in a random coil between η-4 and β-9. The mean RMSF value was 1.19 Å. In apo-AbFabB, between Lys133-Asp143, Asp276-Gly285, Ala299-Thr306, and Gly333-Val337 fluctuated the most compared to the rest of the protein. These areas mostly consist of random coils. RMSF analysis of apo- and ligand-bound proteins reveals that they all show similar patterns in highly fluctuated regions. The RMSF plot of the complexes and mean RMSF values for 100 ns simulations are given in Supplementary Fig. S6 and Supplementary Table S3.

LigFitProt analyzes show the changes in ligand position based on the aligned position of the protein-ligand complex on the protein backbone. It was observed that the AbFabB-L1 complex had the highest RMSD mean value among all complexes, 4.21 Å, while the AbFabB-L2 complex had the lowest value. The rotational motions of the ligands were also examined. LigFitLig plots show the changes that the ligand makes within itself and how consistent the ligand is. It is calculated by superimposing other ligand positions during molecular dynamics simulation to the initial ligand conformation. Results showed that all compounds had minor rotational motion, and all their RMSD mean values were less than 2.0 Å. The highest RMSD mean value belongs to the L5 with 1.52 Å, and the lowest RMSD mean value belongs to the L3 with 0.23 Å. The mean LigFitProt and LigFitLig RMSD values of the nine compounds throughout the 100 ns simulations are represented in Supplementary Table S3.

Compounds L2, L6, and L7 have been selected for the 1 μs MD simulations for assessing ligand stability during a long simulation time because of having the best free energies and interaction with the key residues. We have also simulated the AbFabB-TLM complex for 1 μs for comparison. At the end of the simulation, MM-GBSA binding free energies were calculated for compounds other than the TLM and L2, which lost their interaction with the receptor and leave the binding site at

approximately 130 ns and 800 ns, respectively.

The RMSD average value of the protein backbone atoms of the AbFabB-TLM complex is higher (2.75 Å) than that of the AbFabB-L6 and AbFabB-L7 complexes and increases especially after the leave of TLM (at 130 ns) and after the 400 ns (Supplementary Figs. S8–A). RMSD plot of the compounds with respect to the protein structure clearly shows that the TLM leaves the protein at about 130 ns while the L6 and L7 keep their binding position in the active site cavity throughout the simulation (Fig. 3C, Supplementary Figs. S8–B). The mean RMSD values for backbone atoms of AbFabB-L6 and AbFabB-L7 complexes were 2.23 Å and 2.24 Å, respectively. Maximum values for AbFabB-L6 and AbFabB-L7 were 3.77 Å and 3.49 Å, while minimum values were 1.01 Å and 0.99 Å, respectively. Towards the end of the simulation, after 964 ns, there are some changes in the complexes' backbones, but the overall plot shows consistent behavior throughout the simulation (Fig. 3A). RMSF plot indicated that the AbFabB-L6 and AbFabB-L7 complexes show similar peaks in the same regions, and minor fluctuations were observed throughout the simulations. While the maximum RMSF value of the AbFabB-L6 complex was 4.81 Å, the maximum RMSF value of AbFabB-L7 was 6.21 Å (Fig. 3B). The highest peak of the plot belongs to residues located between 118 and 145 (Fig. 3B, Supplementary Fig. S7, colored in purple). In the second peak of the RMSF plot, both AbFabB-L6 and AbFabB-L7 complexes showed fluctuation in the loop between β-8 and α-12 which was also found to be highly flexible in ligand bound *E. coli* FabB and responsible for the TLM binding [13,55] (Fig. 3B, Supplementary Fig. S7, colored in blue). The third peak of the plot is seen between Leu296 and Thr306 (Fig. 3B, Supplementary Fig. S7, colored in green). The fourth peak from the RMSF plot is the same for both complexes and the peak began at the end of α-13 (Gly333-Glu336) (Fig. 3B, Supplementary Fig. S7, colored in red). The last peak was in the loop between β-13 and β-14 (407–410) (Fig. 3B, Supplementary Fig. S7, colored in orange). Previous studies showed that the Phe408 (Phe391, Phe392, and Phe393 in *P. aeruginosa, E. coli, and B. melitensis* FabB) plays a vital role in ligand binding and substrate specificity by changing its conformation from closed to open in the apo and intermediate-binding state, respectively (13,22,30,32). Corresponding LigFitProt RMSD mean values for AbFabB-L6 and AbFabB-L7 were 2.66 Å and 1.99 Å. These results suggest that L6 changed its position more, while L7 moved more stable with respect to its initial position (Fig. 3C). AbFabB-L6 and AbFabB-L7 complexes were also evaluated for LigFitLig RMSD values. LigFitLig RMSD plots showed similarities, and mean values for L6 and L7 were 1.14 Å and 1.16 Å, respectively (Fig. 3D).

Compound L6, (2-(6-chloro-9H-carbazol-2-yl)-N-(1H-imidazole-2-yl)propanamide), has imidazole ring and it interacts with aromatic residues Phe212 and Phe408 during most of the simulation time. Hydrophobic interactions with the residues including Phe240, Ala288, and Phe406 were also observed (Fig. 4A). The other moiety of the compound is the polycyclic aromatic hydrocarbon, carbazole, which interacts with Gly407 and His313. Pi-pi stacking interaction was observed between the L6 and catalytic residue His313. L6 also makes a hydrogen bond with His349 but the interactions are not stable until the end of the simulation. His349 makes a water bridge at half of MD simulation time while the other half comprises hydrogen bonding. It was observed that the propanamide moiety of the L6 makes a water bridge with the residue Thr317 (Fig. 4A and B). It was shown that the Thr317 equivalent in *B. melitensis* (Thr300) forms hydrogen bond with the platencin inhibitor [30]. Compound L7, 2-[3-(4-methoxyphenyl)-6-oxo-1.6-dihydropyridazin-1-yl]-N-(1H-1.2.4-triazol-3-yl) acetamide, has methoxyphenyl, 1.6-dihydropyridazin and 1.2.4-triazol ring structures. According to the protein-ligand contact results, L7 makes stable hydrogen bonds with the His313, His349, and Gly407 residues during the simulation. Both His313 and His349 bind to the oxygen of the 1.6-dihydropyridazin ring structure. Gly407 interacts with the acetamide moiety of the compound (Fig. 4C and D). In both ligand-receptor interactions, hydrophobic interaction was observed with active site aromatic residues Phe212, Phe240, Phe406, and Phe408. While L7-Phe406 and Phe408 interactions are not stable until the end of the simulation, L6-Phe408 pi-pi stacking interaction dominates in L6 binding. While the main interaction is the hydrogen bonding in L7 binding, L6 makes mainly hydrophobic interactions. In brief, we have observed that other than the catalytic residues (His313 and His349) Phe406, Gly407, and Phe408 are the key residues involved in the interaction at the malonyl-ACP binding site (Fig. 4). The structure of the protein-ligand complexes before and after the 1 μs molecular dynamics simulations are shown in Fig. 5.

Fig. 6 shows the mean energies contribute to the overall MM-GBSA binding energy. Snapshots from the last 100 ns of the 1 μs MD simulation were taken into account in calculations. While the MM-GBSA ΔG binding energies are very close to each other (−52.72 kcal/mol and −49.39 kcal/mol for L6 and L7, respectively), the main driven forces in binding energies are different. Lipophilic energy, vdW energy, and packing (pi-pi stacking) are the main kinds of energies in L6-protein binding. On the other hand, contributions of coulomb and H-bond energies in L7 are totally different from the L6-protein binding. When the protein-ligand contacts and ΔG binding energy calculations are evaluated together, the L6 interaction has a more non-polar nature compared to the L7.

4. Conclusion

In the WHO's global priority list of pathogens, carbapenem-resistant *Acinetobacter baumannii* is listed as critical. With the benefits of differences between mammalian and bacterial FAS pathways, exploration of

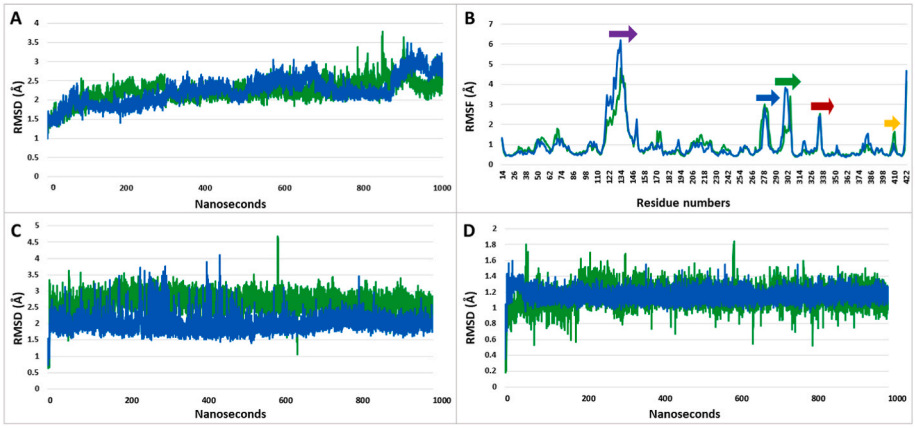

Fig. 3. Plots of AbFabB-L6 and AbFabB-L7 complexes for 1 μs MD simulation. A) RMSD plot. B) RMSF plot. Colored arrows show the most fluctuated parts of the protein during simulations (Supplementary Fig. S7). C) RMSD LigFitProt plot. D) RMSD LigFitLig plot. In all plots, L6 is shown as green, and L7 is shown as blue. (For interpretation of the references to color in this figure legend, the reader is referred to the Web version of this article.)

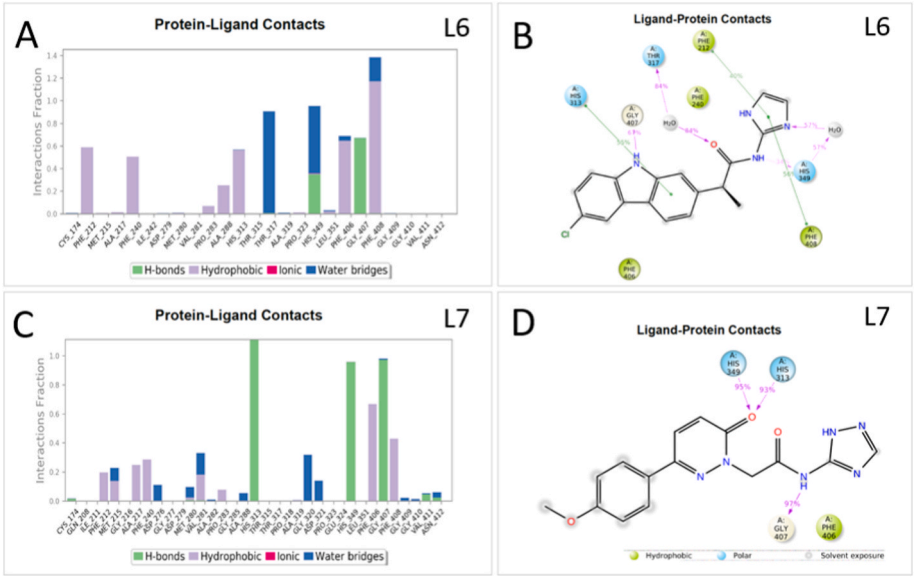

Fig. 4. Protein and ligand contacts for L6 (A and B) and L7 (C and D) during 1 μs MD simulation.

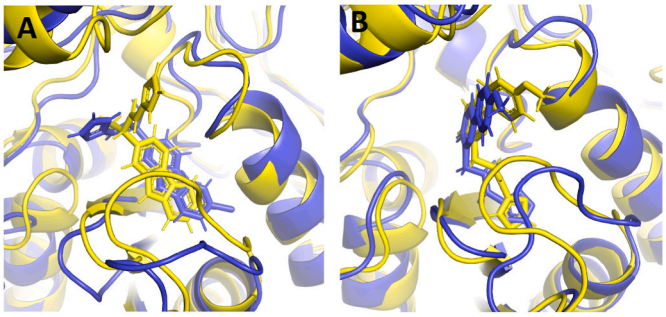

Fig. 5. Superimposition of the initial and the final structures of the protein-ligand complexes. A) AbFabB-L6 initial and the final structure. B) AbFabB-L7 initial and the final structure. The initial structure is shown as yellow, and the final is shown as blue. (For interpretation of the references to color in this figure legend, the reader is referred to the Web version of this article.)

novel drug candidates against bacteria can be carried out by targeting the FAS II pathway without harming human health. Here, we conduct research to screen potential candidates against AbFabB through computational tools. After the 3D structure modeling and docking campaigns, molecular dynamics simulations were performed to assess interaction and ligand stability in the active site of the protein. Binding free energies were analyzed by the MM-GBSA approach. As a result, two of the nine compounds showed lower binding free energies and remained stable throughout the simulation time of 1 μs. In conclusion, these compounds can be considered promising inhibitors for AbFabB. Furthermore, we believe that with *in vitro* studies supporting the findings, a major step will be taken to find novel hit compounds against multidrug-resistant *Acinetobacter baumannii*.

Author contributions

Esra Albayrak: Investigation; Visualization; Writing - Original Draft.
Sinem Koçer: Investigation; Visualization; Writing - Original Draft.
Ozal Mutlu: Conceptualization; Methodology; Investigation; Visualization; Writing - Original Draft.

Declaration of competing interest

The authors declare that they have no known competing financial interests or personal relationships that could have appeared to influence the work reported in this paper.

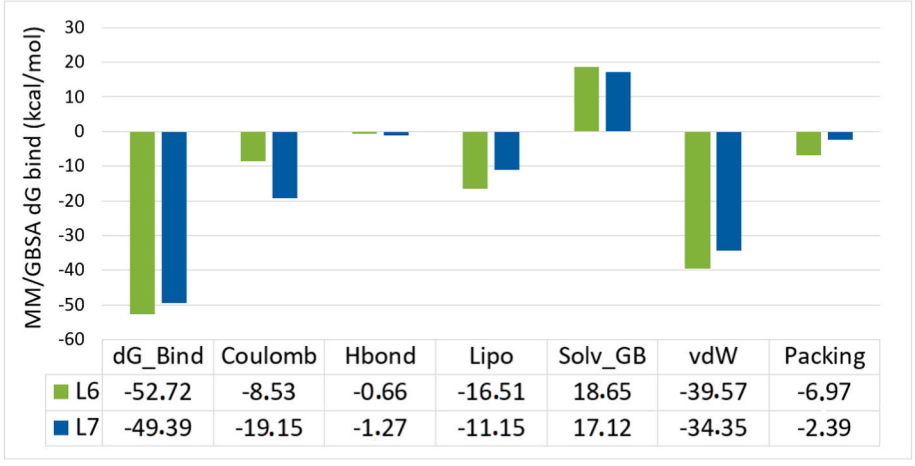

	dG_Bind	Coulomb	Hbond	Lipo	Solv_GB	vdW	Packing
L6	-52.72	-8.53	-0.66	-16.51	18.65	-39.57	-6.97
L7	-49.39	-19.15	-1.27	-11.15	17.12	-34.35	-2.39

Fig. 6. Mean MM-GBSA ΔG values for compounds L6 and L7 and contributions of the various energies (values are kcal/mol).

Data availability

No data was used for the research described in the article.

Appendix A. Supplementary data

Supplementary data to this article can be found online at https://doi.org/10.1016/j.jmgm.2023.108565.

References

[1] J. O'Neill, Review on Antimicrobial Resistance. Tackling Drug-Resistant Infections Globally: Final Report and Recommendations, HM Government and Wellcome Trust, London, 2016, 2016, https://amr-review.org/sites/default/files/160525_Final%20paper_with%20cover.pdf. (Accessed 9 December 2021).

[2] E.M. Cross, F.G. Adams, J.K. Waters, D. Aragão, B.A. Eijkelkamp, J.K. Forwood, Insights into *Acinetobacter baumannii* fatty acid synthesis 3-oxoacyl-ACP reductases, Sci. Rep. 11 (1) (2021) 7050, https://doi.org/10.1038/s41598-021-86400-1.

[3] D. van Duin, D.L. Paterson, Multidrug-resistant bacteria in the community: trends and lessons learned, Infect. Dis. Clin. 30 (2) (2016) 377–390, https://doi.org/10.1016/j.idc.2016.02.004.

[4] World Health Organization, WHO Priority Pathogens List for R&D of New Antibiotics, 2017. https://www.who.int/news/item/27-02-2017-who-publishes-list-of-bacteria-for-which-new-antibiotics-are-urgently-needed. (Accessed 9 December 2021).

[5] L.B. Rice, Federal funding for the study of antimicrobial resistance in nosocomial pathogens: no ESKAPE, J. Infect. Dis. 197 (8) (2008) 1079–1081, https://doi.org/10.1086/533452.

[6] Centers for Disease Control and Prevention, Antibiotic Resistance Threats in the United States, U.S. Department of Health and Human Services, CDC, Atlanta, GA, 2019. https://www.cdc.gov/drugresistance/biggest-threats.html. (Accessed 9 December 2021).

[7] European Centre for Disease Prevention and Control, Carbapenem-resistant *Acinetobacter Baumannii* in Healthcare Settings, ECDC, Stockholm, 2016. https://www.ecdc.europa.eu/sites/default/files/media/en/publications/Publications/8-Dec-2016-RRA-Acinetobacter%20baumannii-Europe.pdf. (Accessed 9 December 2021).

[8] C. Ma, S. McClean, Mapping global prevalence of *Acinetobacter baumannii* and recent vaccine development to tackle it, Vaccines 9 (6) (2021) 570, https://doi.org/10.3390/vaccines9060570.

[9] E.S. Özgür, E.S. Horasan, K. Karaca, G. Ersöz, S. Naycı Atış, A. Kaya, Ventilator-associated pneumonia due to extensive drug-resistant *Acinetobacter baumannii*: risk factors, clinical features, and outcomes, Am. J. Infect. Control 42 (2) (2014) 206–208, https://doi.org/10.1016/j.ajic.2013.09.003.

[10] E. Bergogne-Bérézin, K.J. Towner, Acinetobacter spp. as nosocomial pathogens: microbiological, clinical, and epidemiological features, Clin. Microbiol. Rev. 9 (2) (1996) 148–165, https://doi.org/10.1128/CMR.9.2.148.

[11] Y.M. Zhang, S.W. White, C.O. Rock, Inhibiting bacterial fatty acid synthesis, J. Biol. Chem. 281 (26) (2006) 17541–17544, https://doi.org/10.1074/jbc.R600004200.

[12] H.J. Janßen, A. Steinbüchel, Fatty acid synthesis in *Escherichia coli* and its applications towards the production of fatty acid based biofuels, Biotechnol. Biofuels 7 (1) (2014) 7, https://doi.org/10.1186/1754-6834-7-7.

[13] A.C. Price, K.H. Choi, R.J. Heath, Z. Li, S.W. White, C.O. Rock, Inhibition of beta-ketoacyl-acyl carrier protein synthases by thiolactomycin and cerulenin. Structure and mechanism, J. Biol. Chem. 276 (9) (2001) 6551–6559, https://doi.org/10.1074/jbc.M007101200.

[14] J.E. Cronan, J. Thomas, Bacterial fatty acid synthesis and its relationships with polyketide synthetic pathways, Methods Enzymol. 459 (2009) 395–433, https://doi.org/10.1016/S0076-6879(09)04617-5.

[15] W. Huang, J. Jia, P. Edwards, K. Dehesh, G. Schneider, Y. Lindqvist, Crystal structure of beta-ketoacyl-acyl carrier protein synthase II from *E.coli* reveals the molecular architecture of condensing enzymes, EMBO J. 17 (5) (1998) 1183–1191, https://doi.org/10.1093/emboj/17.5.1183.

[16] S. Kauppinen, M. Siggaard-Andersen, P. von Wettstein-Knowles, beta-Ketoacyl-ACP synthase I of *Escherichia coli*: nucleotide sequence of the fabB gene and identification of the cerulenin binding residue, Carlsberg Res. Commun. 53 (6) (1988) 357–370, https://doi.org/10.1007/BF02983311.

[17] X. Qiu, C.A. Janson, A.K. Konstantinidis, S. Nwagwu, C. Silverman, W.W. Smith, S. Khandekar, J. Lonsdale, S.S. Abdel-Meguid, Crystal structure of beta-ketoacyl-acyl carrier protein synthase III. A key condensing enzyme in bacterial fatty acid biosynthesis, J. Biol. Chem. 274 (51) (1999) 36465–36471, https://doi.org/10.1074/jbc.274.51.36465.

[18] J.D. Nanson, Z. Himiari, C.M. Swarbrick, J.K. Forwood, Structural characterisation of the beta-ketoacyl-acyl carrier protein synthases, FabF and FabH, of *Yersinia pestis*, Sci. Rep. 5 (2015), 14797, https://doi.org/10.1038/srep14797.

[19] R.J. Heath, S.W. White, C.O. Rock, Lipid biosynthesis as a target for antibacterial agents, Prog. Lipid Res. 40 (6) (2001) 467–497, https://doi.org/10.1016/s0163-7827(01)00012-1.

[20] T.M. Loftus, D.E. Jaworsky, G.L. Frehywot, C.A. Townsend, G.V. Ronnett, M. D. Lane, F.P. Kuhajda, Reduced food intake and body weight in mice treated with fatty acid synthase inhibitors, Science 288 (5475) (2000) 2379–2381, https://doi.org/10.1126/science.288.5475.2379.

[21] P.R. Deepa, S. Vandhana, S. Muthukumaran, V. Umashankar, U. Jayanthi, S. Krishnakumar, Chemical inhibition of fatty acid synthase: molecular docking analysis and biochemical validation in ocular cancer cells, J. Ocul. Biol. Dis Infor. 3 (4) (2010) 117–128, https://doi.org/10.1007/s12177-011-9065-7.

[22] C.A. Machutta, G.R. Bommineni, S.R. Luckner, K. Kapilashrami, B. Ruzsicska, C. Smmerling, C. Kisker, P.J. Tonge, Slow onset inhibition of bacterial beta-ketoacyl-acyl carrier protein synthases by thiolactomycin, J. Biol. Chem. 285 (9) (2010) 6161–6169, https://doi.org/10.1074/jbc.M109.077909.

[23] J.T. Tsay, C.O. Rock, S. Jackowski, Overproduction of beta-ketoacyl-acyl carrier protein synthase I imparts thiolactomycin resistance to *Escherichia coli* K-12, J. Bacteriol. 174 (2) (1992) 508–513, https://doi.org/10.1128/jb.174.2.508-513.1992.

[24] S. Jackowski, Y.M. Zhang, A.C. Price, S.W. White, C.O. Rock, A missense mutation in the fabB (beta-ketoacyl-acyl carrier protein synthase I) gene confers thiolactomycin resistance to *Escherichia coli*, Antimicrob. Agents Chemother. 46 (5) (2002) 1246–1252, https://doi.org/10.1128/AAC.46.5.1246-1252.2002.

[25] J. Wang, S.M. Soisson, K. Young, W. Shoop, S. Kodali, A. Galgoci, R. Painter, G. Parthasarathy, Y.S. Tang, R. Cummings, S. Ha, K. Dorso, M. Motyl, H. Jayasuriya, J. Ondeyka, K. Herath, C. Zhang, L. Hernandez, J. Allocco, A. Basilio, J.R. Tormo, O. Genilloud, F. Vicente, F. Pelaez, L. Colwell, S.H. Lee, B. Michael, T. Felcetto, C. Gill, L.L. Silver, J.D. Hermes, K. Bartizal, J. Barrett, D. Schmatz, J.W. Becker, D. Cully, S.B. Singh, Platensimycin is a selective FabF inhibitor with potent antibiotic properties, Nature 441 (7091) (2006) 358–361, https://doi.org/10.1038/nature04784.

[26] J. Wang, S. Kodali, S.H. Lee, A. Galgoci, R. Painter, K. Dorso, F. Racine, M. Motyl, L. Hernandez, E. Tinney, S.L. Colletti, K. Herath, R. Cummings, O. Salazar, I. González, A. Basilio, F. Vicente, O. Genilloud, F. Pelaez, H. Jayasuriya, K. Young, D.F. Cully, S.B. Singh, Discovery of platencin, a dual FabF and FabH inhibitor with *in vivo* antibiotic properties, Proc. Natl. Acad. Sci. U.S.A. 104 (18) (2007) 7612–7616, https://doi.org/10.1073/pnas.0700746104.

[27] E. Martens, A.L. Demain, Platensimycin and platencin: promising antibiotics for future application in human medicine, J. Antibiot. 64 (11) (2011) 705–710, https://doi.org/10.1038/ja.2011.80.

[28] A.S. Halavaty, Z. Wawrzak, O. Onopriyenko, S. Peterson, A. Savchenko, W.F. Anderson, 1.84 Angstrom Resolution Crystal Structure of 3-oxoacyl-(acyl Carrier Protein) Synthase I (fabB) from *Yersinia pestis* CO92, (to be published).

[29] Y.M. Zhang, M.S. Rao, R.J. Heath, A.C. Price, A.J. Olson, C.O. Rock, S.W. White, Identification and analysis of the acyl carrier protein (ACP) docking site on beta-ketoacyl-ACP synthase III, J. Biol. Chem. 276 (11) (2001) 8231–8238, https://doi.org/10.1074/jbc.M008042200.

[30] E.I. Patterson, J.D. Nanson, J. Abendroth, C. Bryan, B. Sankaran, P.J. Myler, J. K. Forwood, Structural characterization of β-ketoacyl ACP synthase I bound to platencin and fragment screening molecules at two substrate binding sites, Proteins 88 (1) (2020) 47–56, https://doi.org/10.1002/prot.25765.

[31] J. Hou, M. Grabowski, M. Cymborowski, H. Zheng, D.R. Cooper, W.F. Anderson, W. Minor, Center for Structural Genomics of Infectious Diseases (CSGID) "Structure of Beta-Ketoacyl-ACP Synthase I (FabB) from *Vibrio Cholerae*", (to be published).

[32] V. Yadrykhins'ky, C. Georgiou, R. Brenk, Crystal structure of *Pseudomonas aeruginosa* FabB C161A, a template for structure-based design for new antibiotics, F1000Res (2021) 10, https://doi.org/10.12688/f1000research.74018.2. Chem Inf Sci-1102.

[33] R.C. Edgar, MUSCLE: multiple sequence alignment with high accuracy and high throughput, Nucleic Acids Res. 32 (5) (2004) 1792–1797, https://doi.org/10.1093/nar/gkh340.

[34] X. Robert, P. Gouet, Deciphering key features in protein structures with the new ENDscript server, Nucleic Acids Res. 42 (2014), https://doi.org/10.1093/nar/gku316 (Web Server issue), W320–W324.

[35] A. Waterhouse, M. Bertoni, S. Bienert, G. Studer, G. Tauriello, R. Gumienny, F. T. Heer, T.A.P. de Beer, C. Rempfer, L. Bordoli, R. Lepore, T. Schwede, SWISS-MODEL: homology modelling of protein structures and complexes, Nucleic Acids Res. 46 (W1) (2018) W296–W303, https://doi.org/10.1093/nar/gky427.

[36] J. Jumper, R. Evans, A. Pritzel, T. Green, M. Figurnov, O. Ronneberger, K. Tunyasuvunakool, R. Bates, A. Žídek, A. Potapenko, A. Bridgland, C. Meyer, S.A. A. Kohl, A.J. Ballard, A. Cowie, B. Romera-Paredes, S. Nikolov, R. Jain, J. Adler, T. Back, S. Petersen, D. Reiman, E. Clancy, M. Zielinski, M. Steinegger, M. Pacholska, T. Berghammer, S. Bodenstein, D. Silver, O. Vinyals, A.W. Senior, K. Kavukcuoglu, P. Kohli, D. Hassabis, Highly accurate protein structure prediction with AlphaFold, Nature 596 (7873) (2021) 583–589, https://doi.org/10.1038/s41586-021-03819-2.

[37] M. Varadi, S. Anyango, M. Deshpande, S. Nair, C. Natassia, G. Yordanova, D. Yuan, O. Stroe, G. Wood, A. Laydon, A. Žídek, T. Green, K. Tunyasuvunakool, S. Petersen, J. Jumper, E. Clancy, R. Green, A. Vora, M. Lutfi, M. Figurnov, A. Cowie, N. Hobbs, P. Kohli, G. Kleywegt, E. Birney, D. Hassabis, S. Velankar, AlphaFold Protein Structure Database: massively expanding the structural coverage of protein-sequence space with high-accuracy models, Nucleic Acids Res. 50 (D1) (2022) D439–D444, https://doi.org/10.1093/nar/gkab1061, 7.

[38] R.A. Laskowski, M.W. MacArthur, D.S. Moss, J.M. Thornton, PROCHECK: a program to check the stereochemical quality of protein structures, J. Appl. Crystallogr. 26 (1993) 283–291, https://doi.org/10.1107/S0021889892009944.

[39] C. Colovos, T.O. Yeates, Verification of protein structures: patterns of nonbonded atomic interactions, Protein Sci. 2 (9) (1993) 1511–1519, https://doi.org/10.1002/pro.5560020916.

[40] M. Wiederstein, M.J. Sippl, ProSA-web: interactive web service for the recognition of errors in three-dimensional structures of proteins, Nucleic Acids Res. 35 (2007), https://doi.org/10.1093/nar/gkm290 (Web Server issue), W407–W410.

[41] D. Eisenberg, R. Lüthy, J.U. Bowie, VERIFY3D: assessment of protein models with three-dimensional profiles, Methods Enzymol. 277 (1997) 396–404, https://doi.org/10.1016/s0076-6879(97)77022-8.
[42] R.A. Laskowski, E.G. Hutchinson, A.D. Michie, A.C. Wallace, M.L. Jones, J. M. Thornton, PDBsum: a Web-based database of summaries and analyses of all PDB structures, Trends Biochem. Sci. 22 (12) (1997) 488–490, https://doi.org/10.1016/s0968-0004(97)01140-7.
[43] R.A. Laskowski, J. Jabłońska, L. Pravda, R.S. Vařeková, J.M. Thornton, PDBsum: structural summaries of PDB entries, Protein Sci. 27 (1) (2018) 129–134, https://doi.org/10.1002/pro.3289.
[44] J. Mistry, S. Chuguransky, L. Williams, M. Qureshi, G.A. Salazar, E.L. L. Sonnhammer, S.C.E. Tosatto, L. Paladin, S. Raj, L.J. Richardson, R.D. Finn, A. Bateman, Pfam: the protein families database in 2021, Nucleic Acids Res. 49 (D1) (2021) D412–D419, https://doi.org/10.1093/nar/gkaa913.
[45] E. Gasteiger, C. Hoogland, A. Gattiker, S. Duvaud, M.R. Wilkins, R.D. Appel, A. Bairoch, Protein identification and analysis tools on the ExPASy server, in: J. M. Walker (Ed.), The Proteomics Protocols Handbook, Springer Protocols Handbooks. Humana Press, 2005, https://doi.org/10.1385/1-59259-890-0:571.
[46] C.A. Lipinski, F. Lombardo, B.W. Dominy, P.J. Feeney, Experimental and computational approaches to estimate solubility and permeability in drug discovery and development settings, Adv. Drug Deliv. Rev. 23 (1–3) (1997) 3–25, https://doi.org/10.1016/S0169-409X(96)00423-1.
[47] C. Lu, C. Wu, D. Ghoreishi, W. Chen, L. Wang, W. Damm, G.A. Ross, M.K. Dahlgren, E. Russell, C.D. Von Bargen, R. Abel, R.A. Friesner, E.D. Harder, OPLS4: improving force field accuracy on challenging regimes of chemical space, J. Chem. Theor. Comput. 17 (7) (2021) 4291–4300, https://doi.org/10.1021/acs.jctc.1c00302.
[48] H.J.C. Berendsen, J.P.M. Postma, W.F. van Gunsteren, J. Hermans, Interaction models for water in relation to protein hydration, in: B. Pullman (Ed.), Intermolecular Forces. The Jerusalem Symposia on Quantum Chemistry and Biochemistry, 14, Springer, Dordrecht, 1981, https://doi.org/10.1007/978-94-015-7658-1_21.
[49] G.J. Martyna, D.J. Tobias, M.L. Klein, Constant pressure molecular dynamics algorithms, J. Chem. Phys. 101 (1994) 4177–4189, https://doi.org/10.1063/1.467468.
[50] R. Yin, B.Y. Feng, A. Varshney, B.G. Pierce, Benchmarking AlphaFold for protein complex modeling reveals accuracy determinants, Protein Sci. 31 (8) (2022) e4379, https://doi.org/10.1002/pro.4379.
[51] A.O. Stevens, Y. He Y, Benchmarking the accuracy of AlphaFold 2 in loop structure prediction, Biomolecules 12 (7) (2022) 985, https://doi.org/10.3390/biom12070985.
[52] V. Scardino, J.I. Di Filippo, C.N. Cavasotto, How good are AlphaFold models for docking-based virtual screening? iScience 26 (1) (2022), 105920 https://doi.org/10.1016/j.isci.2022.105920.
[53] J.G. Olsen, A. Kadziola, P. von Wettstein-Knowles, M. Siggaard-Andrsen, Y. Lindquist, S. Larsen, The X-ray crystal structure of beta-ketoacyl [acyl carrier protein] synthase I, FEBS Lett. 460 (1) (1999) 46–52, https://doi.org/10.1016/s0014-5793(99)01303-4.
[54] J.G. Olsen, A. Kadziola, P. von Wettstein-Knowles, M. Siggaard-Andrsen, S. Larsen, Structures of β-ketoacyl-acyl carrier protein synthase I complexed with fatty acids elucidate its catalytic machinery, Structure 9 (3) (2001) 233–243.
[55] G. Pappenberger, T. Schulz-Gasch, E. Kusznir, F. Müller, M. Hennig, Structure-assisted discovery of an aminothiazole derivative as a lead molecule for inhibition of bacterial fatty-acid synthesis, Acta Crystallogr. D. Biol. Crystallogr. 63 (Pt 12) (2007) 1208–1216. https://doi:10.1107/S0907444907049852.
[56] U. Daood, J.P. Matinlinna, M.R. Pichika, K.K. Mak, V. Nagendrababu, A.S. Fawzy, A quaternaerory ammonium silane antimicrobial triggers bacterial membrane and biofilm destruction, Sci. Rep. 10 (1) (2020), 10970, https://doi.org/10.1038/s41598-020-67616-z.